Efficient CuO/$AgFe_2O_4$/CeO_2 ternary nanocomposites for photocatalytic degradation of methylene blue dye under solar light irradiation

Mahendran Ananthkumar, Pachaimuthu Akilan, Alagesan Kannan and Venkatachalam Chandrasekaran*
Department of Chemistry, Government Arts College (A), Salem-7, Tamil Nadu, INDIA
*chandru_v_m@yahoo.co.in

Abstract

The creation of a ternary nanocomposite has led to significant improvements in optoelectronic characteristics. In this study, individual and combined nanostructures CeO_2, $AgFe_2O_4$, CuO, $AgFe_2O_4$/CeO_2, CuO/CeO_2 and CuO/$AgFe_2O_4$/CeO_2 were synthesized through a sol-gel method coupled with dispersion in a polar solvent. Their structural, morphological and optical behaviors were thoroughly examined using techniques including X-ray diffraction (XRD), Scanning electron microscopy (SEM), UV-visible spectroscopy and Photoluminescence (PL) analysis. The integration of CeO_2, $AgFe_2O_4$ and CuO in the ternary nanocomposite resulted in a notable reduction of the band gap, enhancing its photocatalytic potential. CeO_2 contributed to improved light harvesting, while CuO functioned as an electron sink, collectively boosting the composite's optical performance.

Furthermore, the formation of heterojunction interfaces among CuO, $AgFe_2O_4$ and CeO_2 promoted efficient separation of photogenerated electron-hole pairs, thus enhancing the catalytic activity of the composite in light-driven reactions. Among the tested samples, the CuO/$AgFe_2O_4$/CeO_2 ternary nanocomposite demonstrated superior photocatalytic efficiency, achieving up to 98% degradation of methylene blue dye within 70 minutes.

Keywords: CuO/$AgFe_2O_4$/CeO_2 ternary nanocomposites, photocatalysis, nanocomposites, methylene blue dye.

Introduction

Semiconductor-based metal oxide photocatalysis has emerged as a highly efficient, eco-friendly and sustainable strategy for the removal of hazardous organic pollutants from wastewater. This approach is cost-effective and operates by breaking down the molecular structure of organic compounds, effectively converting toxic dyes into harmless byproducts with impressive degradation performance[2,3]. Although conventional treatment methods such as physical, chemical and biological processes have been employed for dye degradation, they often suffer from drawbacks like high operational expenses and limited efficiency. In comparison, photocatalytic treatment offers a more straightforward and efficient alternative for purifying water contaminated with organic substances[8,23]. A wide range of semiconductor materials including ferric oxide (Fe_2O_3), titanium dioxide (TiO_2), cuprous oxide (CuO), zinc oxide (ZnO) and cerium oxide (CeO_2) have been extensively investigated for their photocatalytic potential[27]. Among these, CeO_2 nanoparticles have gained considerable attention due to their broad band gap, which contributes to a lower rate of electron-hole recombination. Their surface properties are highly adaptable and they exhibit strong redox characteristics, both of which are essential for effective oxidative and reductive degradation of pollutants[28]. A distinctive attribute of CeO_2 is its outstanding oxygen storage capability, which significantly boosts its catalytic performance. Moreover, its ability to alternate between Ce^{3+} and Ce^{4+} oxidation states imparts versatile redox functionality[18].

However, CeO_2 does have limitations: its large band gap restricts light absorption mainly to the UV region, which hampers efficient utilization of solar energy. Additionally, the tendency of CeO_2 nanoparticles to aggregate reduces their surface area, thus negatively affecting photocatalytic activity[22].

Copper oxide nanoparticles (CuO NPs), on the other hand, are considered promising catalysts for degrading organic dyes due to several advantageous features, such as a relatively narrow band gap (1.2–3.5 eV), low toxicity, natural abundance and economical synthesis methods[20]. Their capacity to adsorbed molecular oxygen plays a key role in suppressing electron-hole recombination, which enhances photocatalytic performance. Under UV irradiation, CuO NPs can initiate reactions that contribute to the breakdown of various pollutants[1]. When combined with CeO_2, the nanostructured CuO-CeO_2 composites especially at lower CuO concentrations exhibit improved synergistic effects[9].

Compared to other systems, the Cu_2O-CeO_2 binary composites show superior light absorption, faster charge transport and more efficient electron transfer, particularly under visible light exposure[29] to catalyze the conversion of CO_2 into ethanol. In these configurations, CeO_2 enhances photon absorption, CuO aids in charge carrier trapping and the heterojunction facilitates effective separation of photogenerated charges[24].

Silver ferrite ($AgFe_2O_4$), a spinel-structured ferrite incorporating Ag^+ ions into an iron oxide matrix, displays both semiconducting and magnetic properties, making it suitable for visible light-driven photocatalysis and magnetic

recovery[6,11,21]. To enhance its efficiency, $AgFe_2O_4$ is often coupled with other semiconductors such as TiO_2, g-C_3N_4 and ZnO, forming nanocomposites that exhibit superior photocatalytic behavior. These $AgFe_2O_4$-based hybrids are favored due to their strong visible light absorption (attributed to the silver component), magnetic separability, low toxicity and synergistic enhancement when integrated with functional materials[25]. Their primary applications include the degradation of synthetic dyes like methylene blue, rhodamine B and methyl orange, as well as pharmaceutical pollutants such as tetracycline and ibuprofen. They are also effective in removing environmental contaminants like phenols and pesticides from wastewater.

Despite their promise, challenges such as photo-corrosion, silver ion leaching and charge carrier recombination can hinder their effectiveness, especially when structural configurations are not adequately optimized[12]. To overcome these limitations and improve the visible light response of binary composites like $CeO_2/AgFe_2O_4$, incorporating a narrow band gap semiconductor such as CuO is a promising strategy. CuO possesses excellent charge transport capabilities, broad-spectrum light absorption, high chemical stability and a large surface area, making it an effective electron mediator for photocatalytic and energy applications. Additionally, the integration of metal nanoparticles and carbon-based structures such as graphene derivatives further enhances photocatalytic behavior by providing extensive surface area and superior conductivity.

Materials like graphene oxide (GO) promote efficient charge carrier movement and inhibit recombination, thereby improving the overall photocatalytic performance. Recent studies support this direction. Lakshita et al[15] synthesized $Ni_{0.5}Zn_{0.5}Fe_2O_4/CeO_2$/MWCNT ternary nanocomposites and reported notable degradation of organic dyes like rose bengal, attributing the improvement to enhanced charge transport dynamics. Similarly, Mohammad et al[17] fabricated a $CeO_2/CuO/Ag_2CrO_4$ hybrid photocatalyst through electrospinning, calcination and chemical precipitation. This composite demonstrated efficient degradation of dye mixtures (rhodamine B and methylene blue) under visible light, which was ascribed to improved charge separation and transfer through heterojunction formation.

Murugadoss et al[19] also developed CeO_2–CuO–$Cu(OH)_2$ nanocomposites using a straightforward chemical method. Their material exhibited a reduced band gap of 2.64 eV and achieved high photocatalytic degradation rates of 96.4% for fast green and 92.7% for bromophenol blue. Furthermore, Gomathi and co-workers[7] introduced a CeO_2/Fe_2O_3/reduced graphene oxide (r-GO) ternary hybrid catalyst that achieved 90% and 86% degradation efficiencies for methylene blue and methyl orange respectively under UV light and retained its catalytic stability over five reuse cycles.

In the present work, we report the synthesis of CuO/ $AgFe_2O_4/CeO_2$ ternary nanocomposites using a sol-gel and hydrothermal approach combined with a polar solvent dispersion method. The photocatalytic efficiency of this material was tested against methylene blue dye under solar light. The enhanced performance was primarily linked to the effective suppression of photogenerated electron-hole recombination within the ternary structure.

Material and Methods

Materials: The following chemicals were procured from Merck India Pvt. Ltd.: silver nitrate ($AgNO_3$), ferrous sulfate heptahydrate ($FeSO_4 \cdot 7H_2O$), nickel chloride hexahydrate ($NiCl_2 \cdot 6H_2O$), ammonium ceric nitrate ($(NH_4)_2Ce(NO_3)_6$), copper sulfate pentahydrate ($CuSO_4 \cdot 5H_2O$) and ammonium hydroxide (NH_4OH). Double-distilled water was used to prepare the dye solution for photocatalytic studies. To adjust the pH of the dye solution, sodium hydroxide (NaOH) and hydrochloric acid (HCl) were added to simulate basic and acidic conditions, respectively. Triethanolamine (TEOA) ($N(CH_2CH_2OH)_3$), benzoquinone (BQ) ($C_6H_4O_2$) and isopropanol (IPA) (C_3H_8O) were employed as scavengers to identify and quantify the active species involved during photocatalytic activity.

Synthesis of $AgFe_2O_4$: $AgFe_2O_4$ nanoparticles were synthesized using a precipitation method at ambient temperature. Initially, 20 mL of a 5% silver nitrate solution was slowly introduced into 100 mL of double-distilled water in a beaker, followed by magnetic stirring for 30 minutes to ensure uniform dispersion of silver ions. Subsequently, 10 mL of a 10% ferrous sulfate heptahydrate solution was added to the mixture, which was then stirred continuously for 2 hours. The resulting solution was transferred into a Teflon-lined autoclave and subjected to hydrothermal treatment at 180 °C for 24 hours. The obtained solid product was collected by filtration, washed three times with a water-ethanol mixture and dried at 60 °C for 8 hours.

Synthesis of CeO_2 nanoparticles: In a typical synthesis, a clear sol solution was prepared by controlled dissolving of 5 g of ammonium ceric nitrate under vigorous stirring. For chemical homogeneity, 10 ml of an aqueous ammonia solution is added dropwise. The dense gels are filtered and washed with methanol before being used.The mixture underwent a 12 hrs drying process at 120°C to eliminate impurities and water molecules.The powder is heated at 500°C for 4 hours on a Muffle furnace, resulting in the formation of yellow-colored CeO_2 nanoparticles.

Synthesis of CuO: To synthesize CuO, 10% copper sulfate solution was prepared by dissolving the salt in 100 mL of distilled water. This solution was then converted into copper hydroxide by the gradual addition of 1 M ammonium hydroxide (NH_4OH) under vigorous stirring. The resulting precipitate was thoroughly washed with distilled water and dried in a hot air oven at 100 °C to eliminate residual moisture. The dried solid was then ground using a mortar and pestle, followed by calcination at 500 °C for 2 hours to obtain copper oxide (CuO).

Formation of CuO/CeO_2 binary composites: Pure cubic-phase CeO_2 was synthesized and used in the fabrication of CuO/CeO_2 binary composites, incorporating CuO. To prepare the 2 wt% CuO/CeO_2 composite, 0.02 g of CuO was dispersed in 40 mL of ethanol followed by the addition of 0.2750 g of oxalic acid. The mixture was stirred using an electromagnetic stirrer to achieve a uniform suspension. Then, 0.98 g of CeO_2 was introduced into the suspension and the mixture was stirred continuously for 6 hours. The resulting suspension was dried and subsequently annealed at 300 °C for 3 hours in a Muffle furnace. The final product was labeled as 2CuCe. Different ratios of CuO and CeO_2 were also used to synthesize a series of binary composites, all designated with the name 2CuCe, 4CuCe, 6CuCe and 8CuCe.

Preparation of $AgFe_2O_4/CeO_2$ binary composites: To synthesize 4 wt% $AgFe_2O_4/CeO_2$ binary composites, 0.024 g of $AgFe_2O_4$ was first dispersed in 40 mL of ethanol. This dispersion was then combined with 0.2750 g of oxalic acid and stirred using an electromagnetic stirrer to form a uniform suspension. Next, 0.96 g of CeO_2 was added to the mixture and the entire blend was stirred continuously for 6 hours. The resulting suspension was dried in a hot air oven and subsequently annealed at 300 °C for 3 hours in a Muffle furnace. This same method was applied to prepare other binary composites with varying $AgFe_2O_4$ contents specifically 4 wt%, 8 wt%, 12 wt% and 16 wt% which were designated as AgFeCe4, AgFeCe8, AgFeCe12 and AgFeCe16 respectively.

Preparation of $CuO/AgFe_2O_4/CeO_2$ ternary nanocomposites: To synthesize 4 wt% $CuO/AgFe_2O_4/CeO_2$ ternary nanocomposites, 0.04 g of CuO was first dispersed in 40 mL of ethanol. To this dispersion, 0.96 g of $AgFe_2O_4/CeO_2$ binary composite and 0.2750 g of oxalic acid were added. The mixture was stirred using an electromagnetic stirrer until a uniform suspension was achieved. This suspension was continuously agitated for 12 hours, then dried and subjected to annealing at 300 °C for 3 hours in a Muffle furnace to obtain the final ternary nanocomposite. Using the same procedure, ternary composites containing 8 wt%, 12 wt% and 16 wt% of CuO were also prepared by adjusting the CuO-to-binary composite ratio accordingly.

Evaluation of Photocatalytic Activity: A locally fabricated photocatalytic reactor setup was utilized to evaluate the degradation performance of organic dyes under natural sunlight exposure. The solar light intensity, determined using the ferrioxalate actinometry method, was measured at 1.20×10^{-5} Einstein L^{-1} s^{-1}. The reactor was placed in a uniformly illuminated area, with its temperature regulated by circulating water through the outer jacket to maintain thermal stability. In a standard photocatalytic test, 100 mL of a dye solution (concentration: 50 mg/L) was mixed with 100 mg of the photocatalyst inside the reactor. The degradation process was initiated and changes in dye concentration were tracked using an Elico UV-Vis spectrophotometer by recording absorbance at the dye's maximum wavelength (λ_{max}).

The percentage of degradation was calculated using the following relations:

$$\% \text{ of Degradation} = \left(\frac{C_0 - C}{C_0}\right) \times 100$$

The initial concentration of the dye solution, denoted as C_0, is equal to the remaining concentration of the dye after degradation.

Characterization: X-ray powder diffraction (XRD) images of pigments were obtained using a Philips X'pert-MPD diffractometer with Cu-Kα radiation in the 2θ range of 20-80°. Measurements were conducted with a step size of 0.028 (2θ) at ambient temperature. The compositional phases of the materials were determined by contrasting the simulated X-ray powder patterns with the JCPDS standard. Crystallite sizes were calculated using the Scherrer equation based on peak widths. Surface morphologies and particle sizes were investigated using Scanning electron microscopy (JEOL JSM-6360LV). Diffuse reflectance spectra in the UV-visible range were collected using a Perkin-Elmer Lambda 35 spectrometer, with $BaSO_4$ serving as the reflection standard. The luminescent emission bands of the materials were determined at room temperature using a Perkin-Elmer LS 55 Luminescence spectrophotometer. Fourier-transform infrared (FT-IR) spectra were acquired using a Bruker Vector 22 spectrometer.

Results and Discussion

The $CuO/AgFe_2O_4/CeO_2$ ternary nanocomposites were synthesized using a polar solvent dispersion technique while the individual precursor materials were prepared through sol-gel and hydrothermal methods. This synthesis approach is environmentally friendly, cost-effective and facilitates the formation of crystalline nanostructures with diverse morphologies. The resulting $CuO/AgFe_2O_4/CeO_2$ composites were thoroughly characterized to examine their morphology, crystallite size, optical behavior and molecular structure using various analytical techniques, including X-ray diffraction (XRD), Scanning electron microscopy (SEM), UV-Visible diffuse reflectance spectroscopy (DRS), Photoluminescence (PL) and Fourier-transform infrared spectroscopy (FTIR).

Crystalline structures analysis: Powder X-ray diffraction (XRD) was employed to assess the crystallinity and phase purity of the synthesized photocatalysts. The XRD patterns of the as-prepared materials including pure photocatalysts such as CeO_2, CuO, $AgFe_2O_4$, binary composites ($AgFe_2O_4$/ CeO_2 and CuO/CeO_2) and the ternary CuO/ $AgFe_2O_4/CeO_2$ nanocomposites are presented in figure 1.

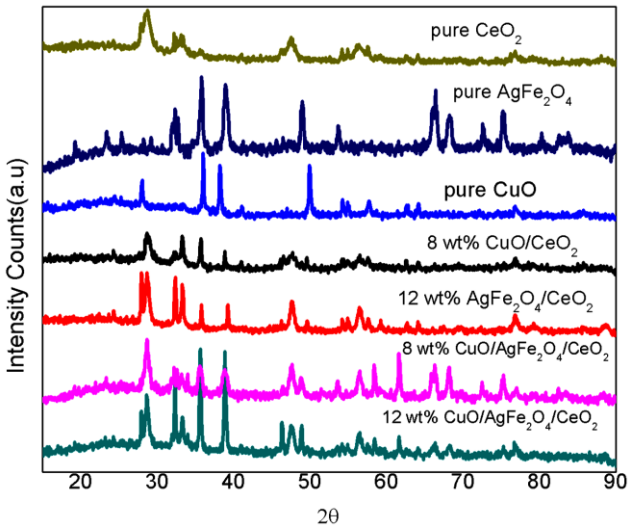

Figure 1: XRD patterns of pure (CeO_2, CuO, $AgFe_2O_4$), binary ($AgFe_2O_4/CeO_2$ and CuO/CeO_2 composites) and $CuO/AgFe_2O_4/CeO_2$ ternary nanocomposites.

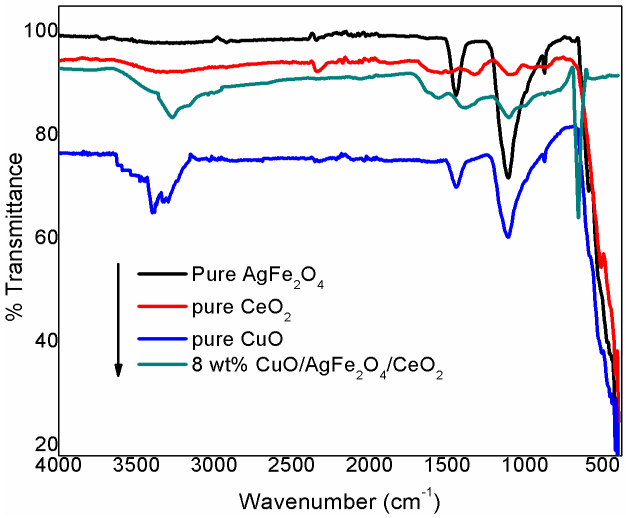

Figure 2: FTIR spectrs of CeO_2 $AgFe_2O_4$ CuO and CuO/ $AgFe_2O_4/CeO_2$ ternary nanocomposites

The diffraction peaks observed for $AgFe_2O_4$ correspond well with those reported in JCPDS card No. 00-032-0369, confirming its spinel cubic crystalline structure. No additional peaks were detected, indicating the absence of impurities. The CeO_2 nanoparticles exhibited prominent peaks at 2θ values of 28.36°, 33.01°, 47.38°, 56.21° and 59.14° which are in agreement with the cubic fluorite structure of CeO_2, as indexed in JCPDS card No. 75-0076. Similarly, the diffraction peaks of CuO matched those listed in JCPDS card No. 45-0937, confirming the successful synthesis of the monoclinic phase. The presence of NiO was also identified, characterized by its monoclinic crystalline phase based on its diffraction profile.

In the 8 wt% CuO/CeO_2 binary composite, the XRD pattern closely resembled that of CeO_2, though with much weaker intensity peaks at approximately 2θ = 35.74° and 38.79°, attributed to the lower CuO content. In contrast, the $AgFe_2O_4/CeO_2$ binary composite showed more distinct reflections corresponding to $AgFe_2O_4$ along with some CeO_2 peaks. In the ternary $CuO/AgFe_2O_4/CeO_2$ nanocomposites, additional weak peaks appeared at 2θ = 35.74°, 38.79°, 35.83° and 39.83°, corresponding to the characteristic planes of $AgFe_2O_4$ and CuO, confirming the successful integration of all three components. The results are explained by the comparatively modest diffraction intensity brought on by the little amounts of CuO and $AgFe_2O_4$. The ternary XRD pattern showed no signs of an impurity phase[26]. As a result, the three-phase composition of the ternary hybrid composites could be verified.

Molecular Interaction Analysis: The FT-IR spectra recorded in the range of 400–4000 cm^{-1} (Figure 2) confirm the presence of functional groups in CeO_2, $AgFe_2O_4$, CuO and the $CuO/AgFe_2O_4/CeO_2$ ternary nanocomposites. A broad absorption band observed around 3369 cm^{-1} corresponds to the O–H stretching vibrations, which are typically attributed to surface hydroxyl groups or adsorbed water molecules. Strong absorption bands appearing near 1380 and 1520 cm^{-1} are associated with the Ce–O–Ce vibrational modes.

In the FT-IR spectra of both CeO_2 and the $CuO/AgFe_2O_4/CeO_2$ ternary nanocomposites, a noticeable band near 663 cm^{-1} is assigned to the stretching vibrations of metal–oxygen bonds, specifically Cu–O, Ce–O and Ag–O linkages[10]. Moreover, the $CuO/AgFe_2O_4/CeO_2$ spectra show a peak at 1089 cm^{-1} which is attributed to the O–W–O stretching vibration. These spectral features suggest the successful formation of ternary nanocomposites incorporating multiple metal oxides, particularly those involving CeO_2 as a matrix material.

Surface properties analysis: The morphology and dispersion of the photocatalysts were examined using scanning electron microscopy (SEM). Figures 3 (a, b and c) present the SEM images of pure CeO_2, $AgFe_2O_4$ and CuO which exhibit distinct surface morphologies such as spongy structures for CeO_2, irregular granular formations for $AgFe_2O_4$ and a shrunken, molten-like surface for CuO. The SEM images of 8 wt% CuO/CeO_2 and 12 wt% $AgFe_2O_4/CeO_2$ binary composites are shown in figure 3 (d and e).

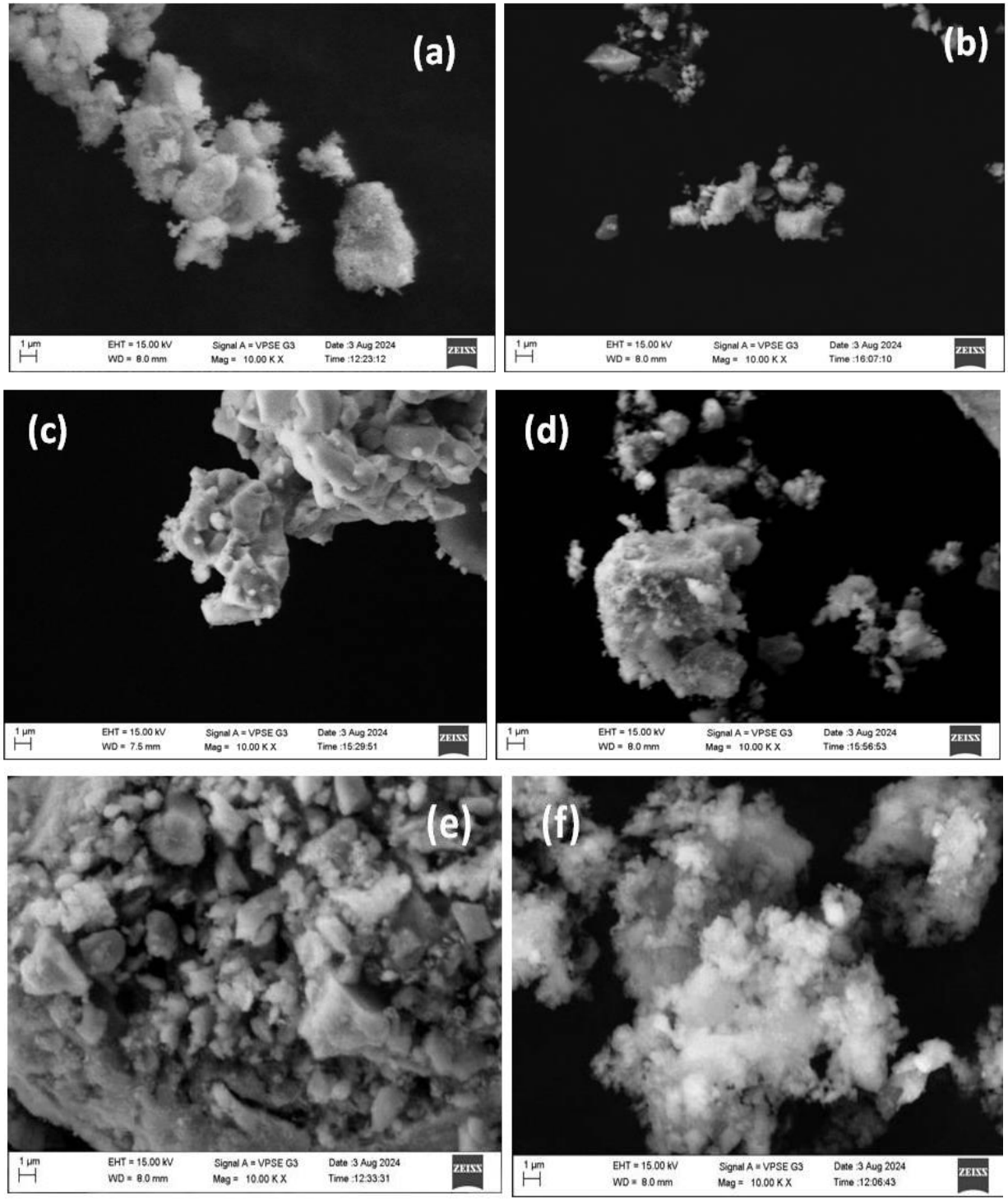

Figure 3: SEM images of (a) pure CeO_2, (b) $AgFe_2O_4$, (c) CuO (d) 8 wt% CuO/CeO_2 (e) 12wt% $AgFe_2O_4/CeO_2$ composites and (f) 12wt% $CuO/AgFe_2O_4/CeO_2$ ternary nanocomposites.

These composites consist of bulky structures formed by the agglomeration of irregularly shaped particles. Each binary nanocomposite displays a unique surface morphology, suggesting that the interaction between different semiconductors and the CeO_2 matrix leads to distinct structural features. Figure 3(f) shows the SEM image of the 12 wt% $CuO/AgFe_2O_4/CeO_2$ ternary nanocomposite. Compared to the binary composites and pure CeO_2, the ternary system exhibits a noticeably different morphology, described as a cloud-like surface texture. This suggests that CuO and $AgFe_2O_4$ are well dispersed within the CeO_2 matrix. Although a clearly defined morphology is not evident in the ternary structure, this type of surface architecture may still be favorable for photocatalytic applications, particularly in the degradation of textile dyes.

Crystalline nature Analysis: Transmission electron microscopy (TEM) was used to examine the size and distribution of CuO and $AgFe_2O_4$ particles on the CeO_2 matrix (Figure 4). The TEM image of the 12 wt% $CuO/AgFe_2O_4/CeO_2$ ternary nanocomposites showed particles with a nearly spherical shape, ranging in size from approximately 50 to 100 nm. The individual nanoparticles of CuO, $AgFe_2O_4$ and CeO_2 exhibited an average size of about 50 nm. These results are consistent with the crystallite size values obtained from XRD analysis and the particle size distribution of CuO and $AgFe_2O_4$ appeared to be quite narrow, centered around 50 nm.

The selected area electron diffraction (SAED) pattern of the synthesized 12 wt% $CuO/AgFe_2O_4/CeO_2$ composite is shown in figure 4(d). The presence of concentric rings composed of faint, fine spots is indicative of polycrystalline CeO_2, while the intense, well-defined diffraction spots correspond to the highly crystalline nature of the CuO and $AgFe_2O_4$ nanoparticles[13].

Optical Properties analysis: The photocatalytic activity of a semiconductor material is largely influenced by its photoresponse, which is determined by its band gap energy. The optical absorption behavior of the synthesized materials was analyzed using UV–Vis diffuse reflectance spectroscopy (DRS), as shown in figure 5. CuO demonstrated strong absorption across both the UV and visible regions (200–750 nm). In contrast, pure CeO_2, being a wide band gap semiconductor, exhibited significant absorption in the UV region but minimal response beyond 400 nm in the visible range. The $AgFe_2O_4$ sample showed a primary absorption peak in the UV region along with a secondary peak around 550 nm, indicating its capability to absorb light in both the UV and visible regions effectively.

The $CuO/AgFe_2O_4/CeO_2$ ternary nanocomposites largely shift to in the range of visible light absorption (372 to 752 nm). In comparison with the undoped-CeO_2 and $AgFe_2O_4/CeO_2$ binary composites, $CuO/AgFe_2O_4/CeO_2$ ternary nanocomposites showed a red shift in absorption edge, indicating the CuO coating on $AgFe_2O_4/CeO_2$ composites. This result is advantageous to broaden the response region of $CuO/AgFe_2O_4/CeO_2$ ternary nanocomposites to visible light and to use solar light as light source in the degradation of dye wastewater[15,17].

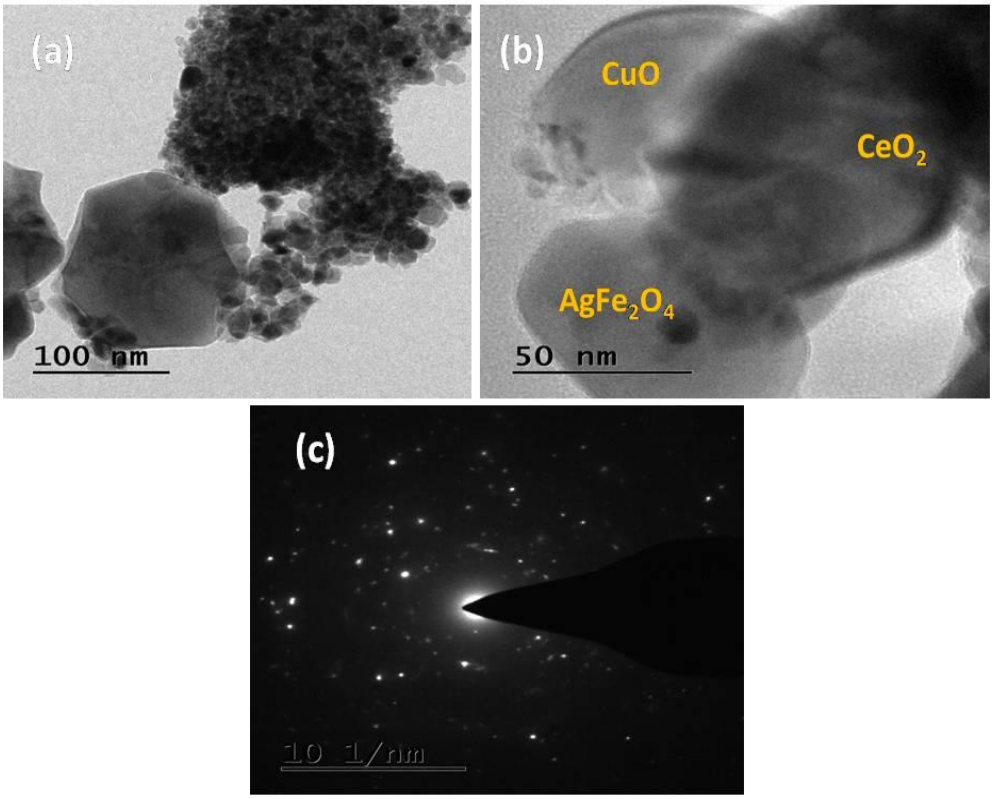

Figure 4: TEM images and SAED pattern of 12wt% $CuO/AgFe_2O_4/CeO_2$ ternary nanocomposites

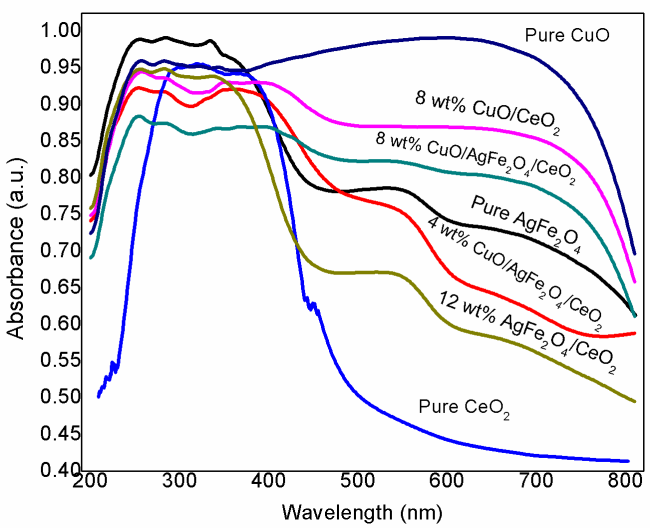

Figure 5: UV-vis DRS of pure (CeO_2, CuO, $AgFe_2O_4$), binary ($AgFe_2O_4/CeO_2$ and CuO/CeO_2 composites) and $CuO/AgFe_2O_4/CeO_2$ ternary nanocomposites.

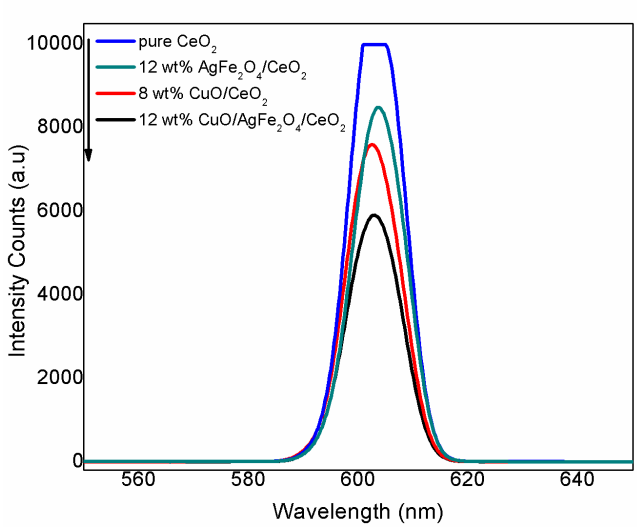

Figure 6: PL spectra of pure CeO_2, 8wt% binary CuO/CeO_2, 12wt% $AgFe_2O_4/CeO_2$ composites, 12wt% CuO/ $AgFe_2O_4/CeO_2$ ternary nanocomposites

Optical Properties analysis: The charge separation efficiency in the prepared materials was investigated using photoluminescence (PL). Photoluminescence (PL) emission typically results from the recombination of photogenerated electron–hole pairs, releasing the absorbed photoenergy. Therefore, higher PL intensity is generally indicative of a greater recombination rate. Figure 6 presents the PL emission spectra of pure CeO_2, 8 wt% CuO/CeO_2, 12 wt% $AgFe_2O_4/CeO_2$ binary composites and 12 wt% CuO/ $AgFe_2O_4/CeO_2$ ternary nanocomposites. All measurements were conducted at room temperature with an excitation wavelength of 380 nm. Each sample displayed an emission peak at 602 nm, corresponding to the radiative recombination of electrons and holes.

The PL intensity for both 8 wt% CuO/CeO_2 and 12 wt% $AgFe_2O_4/CeO_2$ composites was lower than that of pure CeO_2, indicating reduced electron–hole recombination. Among all the samples, the 12 wt% $CuO/AgFe_2O_4/CeO_2$ ternary nanocomposite exhibited the lowest PL intensity, suggesting a more efficient suppression of charge carrier recombination. These findings imply that the combined effect of CuO and $AgFe_2O_4$ on the CeO_2 matrix enhances charge separation and extends the lifetime of photogenerated carriers. The decreased PL intensity of the ternary composite supports its improved photocatalytic performance for dye degradation.

Photocatalytic Studies

Photodegradability of methylene blue dye: Figure 7 illustrates the photocatalytic performance of various nanocomposites including pure materials (CeO_2, CuO, $AgFe_2O_4$), binary systems ($AgFe_2O_4/CeO_2$ and CuO/CeO_2) and the $CuO/AgFe_2O_4/CeO_2$ ternary nanocomposites, all tested for the degradation of methylene blue (MB) dye under solar irradiation. MB dye was chosen for this study due to its strong absorption in the UV-visible range. According to the UV-visible absorption spectra, a 30 mg/L MB dye solution absorbs approximately 80% of incident light between 550

and 700 nm over 1 cm path length. Therefore, at concentrations above 30 mg/L, complete degradation using a simple photocatalytic method such as with CeO_2 alone becomes more challenging and time consuming.

The binary composites, CuO/CeO_2 and $AgFe_2O_4/CeO_2$, displayed improved photocatalytic activity compared to the individual pure components. It was observed that the photocatalytic degradation of MB dye increased progressively with the incorporation of CuO and $AgFe_2O_4$ into the CeO_2 matrix. Interestingly, the highest degradation efficiencies were achieved with 8 wt% CuO/CeO_2 and 12 wt% $AgFe_2O_4/CeO_2$ composites. However, increasing the content of CuO or $AgFe_2O_4$ beyond these optimal levels resulted in reduced activity, indicating that excess loading may hinder photocatalytic efficiency.

Further studies have explored enhancing CeO_2's photocatalytic response by developing ternary systems with varying CuO loadings on a 12 wt% $AgFe_2O_4/CeO_2$ base under solar light. The goal was to further boost CeO_2's activity. After 70 minutes of solar exposure, the degradation rates for MB dye using 8 wt% CuO/CeO_2 and 12 wt% $AgFe_2O_4/CeO_2$ composites reached only 62% and 65% respectively, reinforcing the importance of optimizing the component ratios for maximum performance.

Under identical experimental conditions, the $CuO/AgFe_2O_4/CeO_2$ ternary nanocomposites demonstrated superior photocatalytic degradation efficiency, ranging from 87% to 99%. Notably, increasing the CuO content to 12 wt% significantly enhanced the photocatalytic performance of the composite, indicating an optimal enhancement in activity at this concentration. However, when the CuO content was further increased to 16 wt%, a decline in degradation efficiency to approximately 83% was observed.

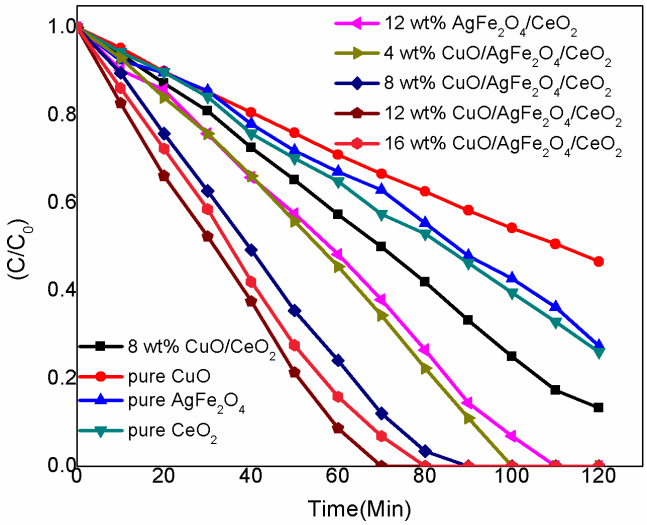

Figure 7: Photocatalytic degradation plots of MB dye over pure CeO_2, CuO, $AgFe_2O_4$, binary ($AgFe_2O_4/CeO_2$ and CuO/CeO_2 composites) and $CuO/AgFe_2O_4/CeO_2$ ternary nanocomposites

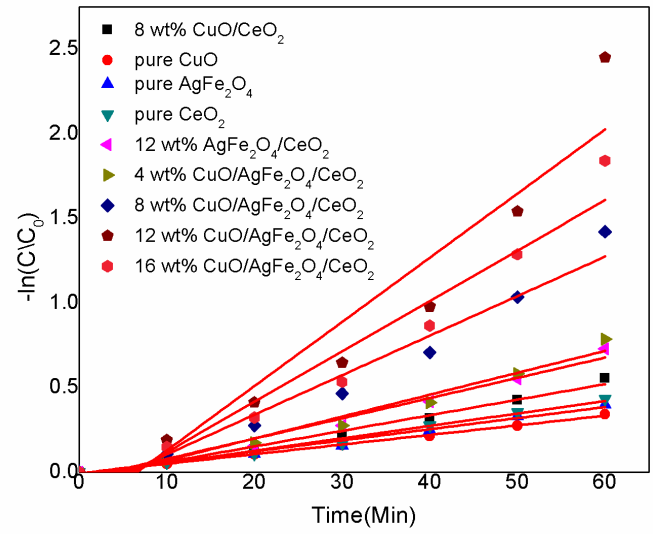

Figure 8: Photocatalytic kinetic plots of MB dye over pure CeO_2, CuO, $AgFe_2O_4$, binary ($AgFe_2O_4/CeO_2$ and CuO/CeO_2 composites) and $CuO/AgFe_2O_4/CeO_2$ ternary nanocomposites

This reduction suggests that excessive CuO may lead to aggregation or surface coverage that inhibits active site accessibility. Therefore, 12 wt% CuO is identified as the optimal loading for achieving maximum photocatalytic efficiency in the $CuO/AgFe_2O_4/CeO_2$ ternary system. Figures 8 illustrates the photocatalytic degradation kinetics of MB dye under the effect of $AgFe_2O_4$, CeO_2, CuO, $AgFe_2O_4/CeO_2$, CuO/CeO_2 and $CuO/AgFe_2O_4/CeO_2$ ternary nanocomposites. The data obtained from the degradation studies were analysed with the Langmuir–Hinshelwood kinetic model:

$$r_s = \frac{kKc}{1+KC}$$

where r_S is the specific degradation reaction rate the dye ($mgl^{-1}min^{-1}$), C the concentration of the dye (mgl^{-1}), k the reaction rate constant (min^{-1}) and K is the dye adsorption constant. When the concentration (C) is small enough, the above equation can be simplified in an apparent pseudo first-order equation:

$$r_s = kKC = K_{app}C\left(=-\frac{dc}{dt}\right)$$

After integration, we will get:

$$-\ln\left(\frac{C}{C_0}\right) = k_{app}\,t$$

where C_0 is the initial concentration ($mg\,l^{-1}$), C is the concentration of the dye after (**t**) minutes of illumination. The data obtained from the degradation of MB dye fits well the apparent pseudo first order kinetics. The electrons in the conduction band can be transferred to surface adsorbed oxygen molecules and form superoxide anions, which can further transform to $OH^{\bullet}$ and initiate the degradation of dye.

Photocatalytic mechanism: The improved visible light absorption and effective charge separation and transfer via many channels, as suggested in figure 9, are two major variables that contribute to the increased sunlight photocatalytic efficiency of $CuO/AgFe_2O_4/CeO_2$ ternary nanocomposites.

To understand the mechanism of electron–hole separation, it is essential to determine the valence band (VB) and conduction band (CB) edge potentials of the synthesized CuO, $AgFe_2O_4$ and CeO_2 materials. These values can be estimated using standard theoretical equations for semiconductor photocatalysts[6]. A potential charge transfer pathway is proposed for the $CuO/AgFe_2O_4/CeO_2$ ternary nanocomposites to explain their enhanced photocatalytic activity (illustrated in figure 10). In this proposed mechanism, CeO_2 serves as a mediator between CuO and $AgFe_2O_4$ during the photocatalytic process.

As shown in figure 9, the VB of CeO_2 (2.56 V) is more positive compared to $AgFe_2O_4$ (2.50 V) and CuO (1.20 V). Additionally, CeO_2 exhibits a CB potential of -0.32 V, which is more negative than that of $AgFe_2O_4$ (-0.05 V) but less negative than CuO (-0.58 V). This allows photogenerated electrons in the CB of CeO_2 to transfer toward $AgFe_2O_4$, while electrons from the CB of CuO can migrate into CeO_2. At the same time, photogenerated holes can move from the VB of CeO_2 to that of $AgFe_2O_4$. This efficient spatial separation of electrons and holes reduces recombination and facilitates the generation of reactive oxygen species, significantly enhancing the photocatalytic degradation of pollutants.

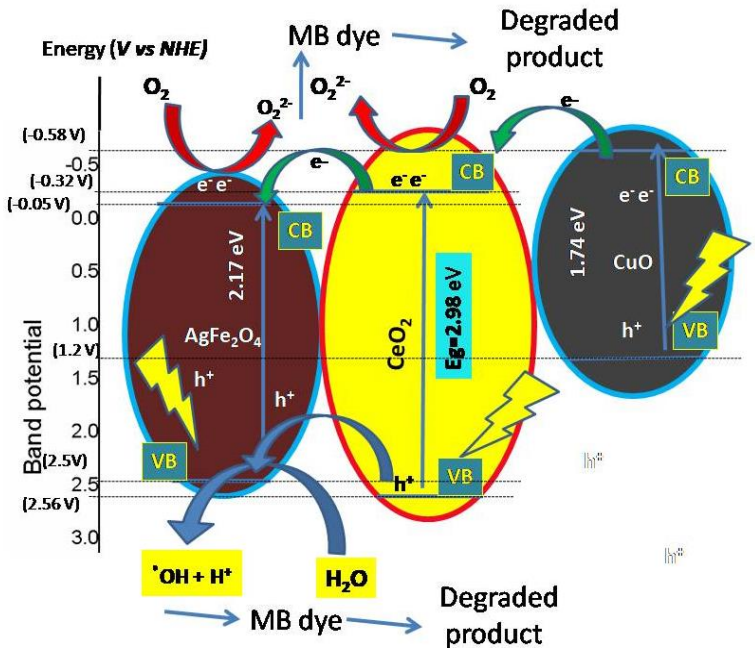

Figure 9: Photoelectron and hole separation mechanism proposed on $CuO/AgFe_2O_4/CeO_2$ ternary nanocomposites

Radical trapping experiments: The effectiveness of a photocatalytic process is largely influenced by the involvement of specific reactive species. To better understand the degradation mechanism of methylene blue (MB) dye, radical scavenging experiments were performed to identify the roles of different active species. The results of these experiments are shown in figure 10. Triethanolamine (TEOA), benzoquinone (BQ) and isopropanol (IPA) were used as scavengers for holes (h^+), superoxide radicals ($\bullet O_2^-$) and hydroxyl radicals (•OH) respectively. These scavengers were selected based on the known significance of these species in the photocatalytic degradation of organic pollutants under solar irradiation[5,14]. For comparison, a control experiment was also conducted without any scavenger (NSC).

As illustrated in figure 10, approximately 98% degradation of MB dye occurred in the absence of scavengers. When BQ and IPA were added, the degradation efficiency dropped to 51% and 39% respectively, indicating the essential roles of superoxide and hydroxyl radicals in the photocatalytic process. The addition of TEOA also led to a reduction in degradation efficiency, down to around 84%, suggesting that holes (h^+) contribute to the degradation but to a lesser extent than radicals. These results confirm that both •OH and $\bullet O_2^-$ are the primary reactive species responsible for the efficient breakdown of MB dye.

Stability and Reusability: To evaluate the stability of the 12 wt% $CuO/AgFe_2O_4/CeO_2$ ternary nanocomposites during photocatalytic processes, recycling experiments were performed by repeatedly degrading methylene blue (MB) dye under solar irradiation across five consecutive cycles. As illustrated in figure 11, the photocatalytic performance of the nanocomposite remained consistently high even after three cycles. A slight decrease in degradation efficiency was observed in the later cycles, which may be attributed to photocatalyst loss or possible catalytic deactivation during the reuse experiments[4].

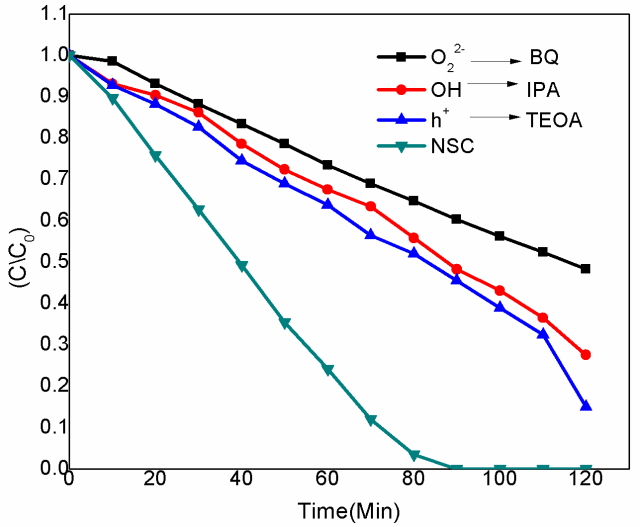

Figure 10: Effect of trapping agents on photocatalytic degradation using 12 % $CuO/AgFe_2O_4/CeO_2$ ternary nanocomposites

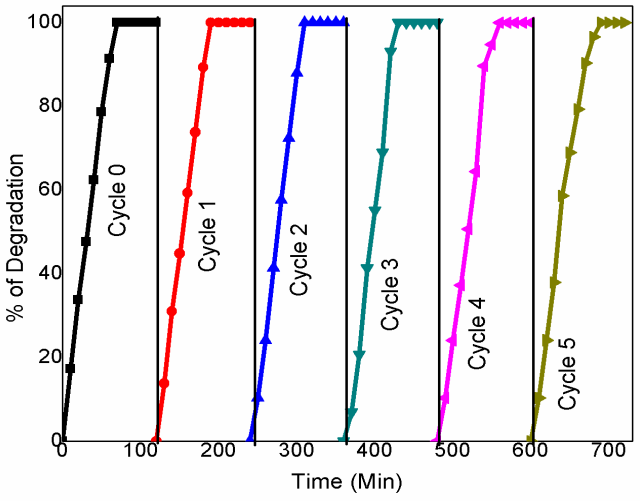

Figure 11: Stability test of 12 % $CuO/AgFe_2O_4/CeO_2$ ternary nanocomposites for five cycles after recycling five times for MB dye degradation

Conclusion

In this study, $CuO/AgFe_2O_4/CeO_2$ ternary nanocomposites were successfully synthesized using a simple ethanol-based dispersion method followed by annealing at 300 °C for three hours. The formation of the ternary nanocomposite was confirmed by PXRD and FT-IR analyses, which showed distinct peaks corresponding to CuO, $AgFe_2O_4$ and CeO_2. SEM imaging revealed that the material exhibited a uniform, fine powder morphology. UV-Vis DRS analysis indicated strong visible light absorption within the 550–750 nm range for the $CuO/AgFe_2O_4/CeO_2$ composite. Furthermore, the PL spectrum showed a relatively weak emission intensity, suggesting reduced recombination of photoinduced charge carriers and efficient electron trapping.

The alignment of the energy band positions among NiO, $AgFe_2O_4$ and CeO_2 further promoted charge separation and transfer. Under sunlight irradiation, the 12 wt% $CuO/AgFe_2O_4/CeO_2$ nanocomposite demonstrated enhanced photocatalytic performance, achieving dye degradation efficiency of up to 99% within 70 minutes, an improvement from the initial 87%. This enhancement is attributed to the presence of CuO and $AgFe_2O_4$, which act as electron traps, minimizing recombination and generating more holes, thereby increasing the formation of hydroxyl radicals that drive the degradation process.

The active species mainly involved in dye degradation were identified as superoxide (O_2^{-}•) and hydroxyl radicals (•OH). Reusability tests confirmed the excellent stability and reusability of the $CuO/AgFe_2O_4/CeO_2$ photocatalyst. This work introduces a promising class of solar-responsive photocatalysts suitable for accelerating the breakdown of textile dyes.

Acknowledgement

The authors express their sincere appreciation to the Department of Chemistry, Periyar University.

References

1. Arif H. et al, Photocatalytic degradation of atrazine and abamectin using Chenopodium album leaves extract mediated copper oxide nanoparticles, *Z. Phys. Chem.*, **237(6)**, 689–705 **(2023)**

2. Arularasu M.V., Begum M.Y., Alamri A. and Fatease A.A., Visible light degradation of antibiotics catalyzed by nanoporous carbon/V_2O_5 nanocomposite: structural, optical and electrochemical properties, *J. Mol. Struct*., **1322**, 140615 **(2025)**

3. Arularasu M.V., Rajendran T.V., Arkook B., Harb M. and Kaviyarasu K., Enhanced electrochemical performance of highly porous CeO_2 -doped Zr nanoparticles for supercapacitor applications, *Microsc. Res. Tech.*, **88**, 621-630 **(2025)**

4. Fangxiao W., Qinfeng X., Rong L. and Chun Y.Z., Flower-like Ag_2WO_4/CeO_2 heterojunctions with oxygen vacancies and expedited charge carrier separation boost the photocatalytic degradation of dyes and drugs, *Dalton Trans*., **51**, 10179-10185 **(2022)**

5. Fathima Khyrun S.M., Jegatha Christy A., Jeyanthinath M. and Suresh S., Photo-triggered antibacterial and catalytic activities of solution combustion synthesized CeO_2/NiO binary nanocomposites, *Inorg. Chem. Comm*., **153**, 110860 **(2023)**

6. Giorgi F., Coglitore D., Curran J.M., Gilliland D., Macko P., Whelan M., Worth A. and Patterson E.A., The influence of inter-particleforces on diffusion at the nanoscale, *Sci. Rep.*, **9**, 12689 **(2019)**

7. Gomathi A., Prabhuraj T., Gokilapriya S., Vasanthi G., Maadeswaran P. and Ramesh Kumar K.A., Design of ternary CeO_2/Fe_2O_3/reduced graphene oxide-based hybrid nanocomposite for superior photocatalytic degradation material for organic dyes, *Dyes and Pigments*, **218**, 111473 **(2023)**

8. Haribaaskar K., Yoganand K.S., Rajendran T.V. and Arularasu M.V., Synthesis of Zr-doped CeO_2 nanoparticles for photocatalytic degradation of methyl orange and electrochemical properties, *Biomass Conv. Bioref.*, Doi: 10.1007/s13399-024-05941-3 **(2024)**

9. Iannaco M.C. et al, CeO_2-CuO composites prepared via supercritical antisolvent precipitation for photocatalytic hydrogen production from lactic acid aqueous solution, *J. CO_2 Util*., **85**, 102878 **(2024)**

10. Jabbar Z.H., Ebrahim S.E. and Ammar S.H., Supported heterogeneous nanocomposites ($SiO_2/Fe_3O_4/Ag_2WO_4$) for visible-light-driven photocatalytic disinfection against *E. coli*, *Mater. Sci. Semicond. Process*, **141**, 106427 **(2022)**

11. Janani B., Abdulaziz A., Al-Kheraif, Thomas A.M., Asad S., Abdallah M., Elgorban, Lija L.R., Arunava D. and Sudheer K., Construction of nano-heterojunction $AgFeO_2$–ZnO for boosted photocatalytic performance and its antibacterial applications, *Mater. Sci. Semicond. Process*, **133**, 105924 **(2021)**

12. Karapetkovska-Hristova Vesna, Treneski Valentino, Pavlović Ivan and Mustafa Syed Khalid, Assessing the Efficacy of Organic and Chemical Treatments for Varroa Mite Control in Macedonian Apiaries, *Res. J. Biotech.*, **19(9)**, 47–55 **(2024)**

13. Khadim H.J., Al-Farraji A. and Ammar S.H., Boosted visible-light-driven photocatalytic degradation of lomefloxacin over α-Ag_2WO_4/NiSx nanocomposites, *Environ. Nanotechnol. Monit. Manag.*, **18**, 100722 **(2022)**

14. Kusum S. et al, Mechanistic insights into the reaction pathway for efficient cationic dye photocatalytic degradation and the importance of the enhanced charge isolation over dual Z-scheme $CeO_2/BiOCl/Ag_2WO_4$ photocatalyst, *J. Water Proc. Eng*., **66(1)**, 105918 **(2024)**

15. Lakshita P., Youssef T., Anurag, Jaideep M., Harita K., Ashok K. and Surjeet C., CeO_2 microspheres/Ni0.5Zn0.5Fe_2O_4/MWCNT ternary hybrid composites for ultrasonic-enhanced photocatalytic wastewater treatment, *Ceram. Int*., **50(19)**, 35600-35608 **(2024)**

16. Mehmet S.N., $AgFe_2O$/MWCNT nanoparticles as novel catalyst combined adsorption-sonocatalytic for the degradation of methylene blue under ultrasonic irradiation, *J. Environ. Chem. Eng.*, **9**, 105207 **(2021)**

17. Mohammad M.S., Hajir K. and Mehrorang G., Enhanced visible light-active CeO2/CuO/Ag2CrO4 ternary heterostructures

based on CeO_2/CuO nanofiber heterojunctions for the simultaneous degradation of a binary mixture of dyes, *New J. Chem.*, **44**, 5033-5048 **(2020)**

18. Mohd I., Md. Mottahir A., Shahir Hussain, Mohammad A.A., Mohd S., Akbar M., Tansir A., Ajeet K. and Kashif I., Highly photocatalytic active r-GO/Fe_3O_4 nanocomposites development for enhanced photocatalysis application: A facile low-cost preparation and characterization, *Ceram. Int*., **47(22)**, 31973-31982 **(2021**)

19. Murugadoss G., Kannappan T., Rajabathar J.R., Manavalan R.K., Salammal S.T. and Venkatesh N., Rapid Photocatalytic Activity of Crystalline CeO_2-CuO-$Cu(OH)_2$ ternary nanocomposite, *Sustainability*, **15**, 15601 **(2023)**

20. Murugan B. et al, Green synthesis of CuO nanoparticles for biological applications, *Inorg. Chem. Commun.*, **155**, 111088 **(2023)**

21. Murugan E., Kaviya M.S., Janakiraman K., Saranya S., Lyric F. and Sathyabarata N.S., Silver ferrite embellished graphene oxide heterogenous nanocomposite for efficient electrochemical detection of gallic acid, *Ind. J. Chem. Technol.*, **29**, 753-759 (**2022)**

22. Nishath A. et al, Facile hydrothermal synthesis of cerium oxide/rGO nanocomposite for photocatalytic and supercapacitor applications, *Appl. Surf. Sci. Adv.*, **11**, 100307 **(2022)**

23. Pushpalatha S., Arularasu M.V., Palanivel C. and Rajendran T.V., Phytoextract-mediated cellulose/CeO_2 nanocomposite for antibacterial and photocatalytic activity, *Biomass Conv. Bioref*., **15**, 3679-3690 **(2025)**

24. Seeharaj P. et al, CeO_2/CuO/TiO_2 heterojunction photocatalysts for conversion of CO_2 to ethanol, *Nanotechnology*, **32**, 375707 **(2021)**

25. Song Z., He Y. and Wang F., A novel z-scheme heterostructured AgI/$AgFeO_2$ composites as an efficient visible-light photocatalyst for the degradation of rhodamine B, *Dig J Nanomater Bios*., **12**, 645–651 **(2017)**

26. Su X., Fan D., Sun H., Yang J., Yu Z., Zhang D., Li H. and Cai P., One-dimensional rod-shaped $Ag_2Mo_2O_7$/BiOI n-n junctions forefficient photodegradation of tetracycline and rhodamine B undervisible light, *J. Alloys Compd.*, **912**, 165184 **(2022)**

27. Sultana S., Mansingh S. and Parida K., Crystal facet and surface defect engineered low dimensional CeO_2 (0D, 1D, 2D) based photocatalytic materials towards energy generation and pollution abatement, *Materials Advances*, **2(21)**, 6942-6983 **(2021)**

28. Sumeet K. and Ashok K., Enhanced photocatalytic activity of rGO-CeO_2 nanocomposites driven by sunlight, *Mat. Sci. Eng.: B*, **223**, 98-108 **(2017)**

29. Zeng S.H., Shui A.Z., Yu H.L. and He C., Rapid synthesis of Cu_2O/CeO_2 p–n heterojunctions with enhanced photocatalytic properties by a sonochemical method, *Int. J. Appl. Ceram. Technol.*, **21**, 3378–3388 **(2024)**.

(Received 09th July 2025, accepted 09th August 2025)